Research Article

Removal of Pb(II) from Aqueous Solutions with Manganese Oxide-Modified Diatomite

Huynh Thanh Danh,[1,2] Nguyen Thi Truc Ly,[3] Vanthan Nguyen,[4] Dinh Quang Khieu ID,[2] and Pham Dinh Du ID[5]

[1]Giong Rieng High School, 91000, Vietnam
[2]University of Sciences, Hue University, 49000, Vietnam
[3]Tan Hiep High School, 91000, Vietnam
[4]Faculty of Automotive Engineering, Ngo Quyen University, 75000, Vietnam
[5]Thu Dau Mot University, 75000, Vietnam

Correspondence should be addressed to Dinh Quang Khieu; dqkhieu@hueuni.edu.vn and Pham Dinh Du; dupd@tdmu.edu.vn

In the present work, natural diatomite modified with manganese oxide (MnO_2) was prepared via direct redox reaction with $KMnO_4$ and HCl. The product was characterized by using X-ray diffraction, Fourier-transform infrared spectroscopy, scanning electron microscopy, transmission electron microscopy, energy-dispersive X-ray, and nitrogen adsorption-desorption isotherms. It was found that the nanorod manganese oxide was highly dispersed onto the diatomite porous matrix. The specific surface area of the obtained manganese oxide/diatomite ($S_{BET} = 68.5 \, m^2 \, g^{-1}$) is larger than that of natural diatomite ($S_{BET} = 55.4 \, m^2 \, g^{-1}$). It was utilized to remove Pb(II) in aqueous solutions. It exhibits an excellent Pb(II) adsorption capacity. The adsorption data fits well with the pseudo-second-order kinetics model, and the adsorption process is endothermic and spontaneous with an activation energy of $41.56 \, kJ \, mol^{-1}$ and follows the Freundlich isotherm model. The Mn/diatomite adsorption capacity for Pb(II) is $81.42 \, mg \, g^{-1}$, calculated with the Langmuir model. In addition, the adsorption mechanism of Pb(II) onto Mn/diatomite is also addressed.

1. Introduction

Heavy metals are commonly found in wastewater from the chemical industry, paints, ceramics, glass, mining, and battery manufacturing and severely harm humans and ecosystems [1, 2]. Among them, lead (Pb(II)) has an amphoteric structure and is a metal with a high toxic level among heavy metals. Pb(II) is easily dispersed through the soil and water ecosystem, and by entering the food chain, it causes toxic effects on human health [3]. Due to exposure to Pb(II) for a long period, the kidneys and immune systems, in particular, can be severely destroyed. Therefore, various methods have been utilized to remove heavy metal ions from aqueous solutions, such as oxidation, coagulation and precipitation, membrane filtration, adsorption, ion exchange, and biologi-

cal treatment [4–9]. Among them, adsorption is the most effective because of its simplicity, low cost, and ability to treat wastewater containing low concentrations of metal ions [10–14].

Diatomite ($SiO_2 \cdot nH_2O$) is a soft, grey, low-density sedimentary rock. The main component of diatomite is the shell of diatoms consisting primarily of amorphous silica. Diatomite has unique properties, such as high porosity, high adsorption capacity, and high heat resistance [15–19]. These properties suggest that diatomite is a potential adsorbent for the pollutants present in industrial wastewater. Furthermore, natural diatomite is abundant, cheap, and environmentally friendly [18]. In Vietnam, diatomite mineral is often applied in shrimp pond treatment, sound and heat insulation, etc. Recently, the modification of diatomite to increase its

applicability has also attracted scientists [20–24]. The modification via hydrothermal process exhibits advantages including nanoparticles with the desired size and shape [25] and formation of a well-crystallized powder [26]. Hence, these techniques have been widely applied to introduce the inorganic compounds with active sites to expand the application of diatomite in adsorption and catalysis [12, 27–30].

Nanoscale manganese oxide (MnO_2) particles, known to be a porous material and a mild oxidant, possess a large surface area and excellent chemical stability in acidic media [31]. Manganese oxide has been widely employed as a constituent material in air batteries [32] and a catalyst for oxygen reduction [33]. In particular, manganese oxide exhibits excellent adsorption toward heavy metals in aqueous sources. However, nanosized MnO_2 particles suffer from heavy agglomeration, limiting their application [34]. Moreover, using pure MnO_2 as an adsorbent is not reasonable regarding economic effectiveness, and it is very difficult to separate the particles from the liquid phase [35]. To deal with these limitations and to promote the treatment efficiency and capabilities for eliminating heavy metals in an aqueous solution with natural diatomite, numerous researchers modified diatomite by coating nanosized MnO_2 particles onto its surface. Al-Degs et al. [10] and Khraished et al. [11] modified diatomite with manganese oxide by treating it with manganese chloride and sodium hydroxide. The results demonstrate that its heavy metal adsorption capacity was much improved compared with that of the original diatomite. The specific surface area of diatomite and Mn/diatomite calculated with the simple and rapid methods was 33 and $80 \, m^2 \, g^{-1}$. The adsorption capacity of diatomite is 24.9, 27.6, and $16.1 \, mg \, g^{-1}$ adsorbates for Pb^{2+}, Cu^{2+}, and Cd^{2+}, respectively, while the corresponding values of Mn/diatomite are 99.0, 57.6, and $27.9 \, mg \, g^{-1}$. Li et al. [36] reported a two-step procedure for diatomite modification with nano-MnO_2, and the material has a maximum adsorption capacity of $56.84 \, mg \, g^{-1}$ for Pb^{2+}. Du et al. [12] also successfully synthesized MnO_2 nanowires on a diatomite substrate. In addition, MnO_2-modified diatomite was also used for Zn(II) adsorption [13], dye adsorption [37], catalysts [38], and electrode modifiers [39].

In this paper, a manganese-modified diatomite material (Mn/diatomite) was prepared with the hydrothermal method via the redox reaction of $KMnO_4$ and HCl, where diatomite was a substrate. The material's physicochemical properties and ability to remove Pb(II) ions from aqueous solutions were investigated.

2. Experimental

2.1. Materials and Chemicals.
Raw diatomite was taken from Phu Yen province, Vietnam, washed several times with water, filtered, dried at 100°C, sieved, and stored in closed containers for further tests. $KMnO_4$ (Merck, Germany), $Pb(CH_3COO)_2 \cdot 3H_2O$, NaOH, HCl, and KCl (Guangdong, China) are of analytical grade and are used without further purification.

2.2. Preparation of Mn/Diatomite.
Diatomite was modified with manganese, according to Wu et al. [40] and Du et al. [12]. Briefly, (i) 0.5 g of diatomite, 5 mmol of $KMnO_4$ (0.79 g), and 80 mL of distilled water were mixed to obtain mixture A; (ii) a certain volume of a 10 M HCl solution was added to mixture A under stirring to obtain mixture B; (iii) the entire mixture B was transferred into a 200 mL Teflon-lined steel autoclave with a quantity of distilled water to fill 80% of the Teflon-flask volume to obtain mixture C; (iv) the Teflon flask was placed in an oven at a specified temperature and for a certain time; and (v) the flask was cooled to ambient temperature, and the solid product was collected, filtered, washed with distilled water, and dried at 60°C for 24 h. The resulting solid is a modified diatomite material and is denoted as Mn/diatomite.

The effects of reaction conditions on the modification, including hydrothermal temperature (80, 120, and 160°C), hydrothermal time (16, 24, and 48 h), and the $KMnO_4$/HCl molar ratio (1 : 1, 1 : 2, 1 : 4, and 1 : 8) were investigated. The details of the experimental conditions used in the diatomite modification are summarized in Table 1.

2.3. Preparation of Nano-MnO₂.
Nano-manganese oxide was prepared according to a similar procedure in Section 2.2. The 10 M HCl solution was added drop-wise (the molar ratio of $KMnO_4$/HCl was adjusted in the ratio of 1 : 1, 1 : 2, 1 : 4, and 1 : 8). The Teflon flask was heated at 160°C for 16 h, and the yielded nano-manganese oxide was dried at 60°C.

2.4. Characterization.
The morphology of the materials was observed by using scanning electron microscopy (SEM, IMS-NKL) with an acceleration voltage of 5 kV and transmission electron microscopy (TEM, EMLab-NIHE) at a voltage of 80 kV. X-ray diffraction (XRD) patterns were recorded on a VNU-D8 Advance Bruker (Germany) powder diffractometer with a Cu Kα radiation source and an angle and time scan step of 0.03° and 0.04 s, respectively. Fourier-transform infrared (FT-IR) spectra were obtained on a Jasco FT/IR-4600 (Japan), with samples being dispersed on KBr pallets and measured within the wavenumber range of 4000-$400 \, cm^{-1}$ with a spectral resolution of $1 \, cm^{-1}$. Nitrogen adsorption measurements were conducted with a Micromeritics Tristar 3000 apparatus at the liquid nitrogen temperature (77 K). The textural properties of the material were examined via the specific surface area and porosity after a heat treatment at 250°C in the N_2 for 5 h. The elemental composition on the material surface was analyzed with energy-dispersive X-ray (EDX) spectroscopy along with the SEM (JEOL JED-2300) at 20 kV. The Pb(II) concentration was determined with the atomic absorption spectroscopy (AAS) method on a Shimadzu AA-7000 (Singapore).

2.5. Adsorption Experiments

2.5.1. Evaluate the Pb(II) Adsorption Capacity of the Material.
A quantity of adsorbent (0.1 g) was placed into an Erlenmeyer flask containing 100 mL of a Pb(II) solution with a prescribed concentration and shaken at ambient temperature for 3 h to achieve adsorption-desorption equilibrium. Then, the solution

TABLE 1: Experimental conditions were carried out during the preparation of the Mn/diatomite samples.

Sample	Mass of diatomite (g)	Mass of KMnO$_4$ (g)	10 M HCl volume (mL)	KMnO$_4$/HCl molar ratio	Hydrothermal temperature (°C)	Hydrothermal time (h)
1	0.5	0.79	4	1:8	80	16
2	0.5	0.79	4	1:8	120	16
3	0.5	0.79	4	1:8	160	16
4	0.5	0.79	0.5	1:1	80	16
5	0.5	0.79	1	1:2	80	16
6	0.5	0.79	2	1:4	80	16
7	0.5	0.79	2	1:4	80	24
8	0.5	0.79	2	1:4	80	48

was filtered to remove the adsorbent, and the Pb(II) ion concentration in the solution was determined.

The adsorption capacity at equilibrium (q_e) was calculated according to the following equation.

$$q_e = \frac{(C_0 - C_e) \times V}{m},$$ (1)

where C_0 and C_e (mg L^{-1}) are the concentration of Pb(II) in the solution at the beginning and at equilibrium, respectively; V (L) is the volume of the Pb(II) solution; and m (g) is the weight of Mn/diatomite used for each adsorption.

2.5.2. Pb(II) Adsorption Kinetics. Mn/diatomite (0.1 g) was placed into a double-necked flask containing 100 mL of the Pb(II) solution with a prescribed concentration under magnetic stirring at a prescribed temperature, under natural pH. At a specified interval, a certain volume of solution was withdrawn and centrifuged to remove the adsorbent, and the Pb(II) concentration in the supernatant was determined with the AAS technique.

The adsorption capacity at time t (q_t) was calculated according to the following equation.

$$q_t = \frac{(C_0 - C_t) \times V}{m},$$ (2)

where C_t (mg L^{-1}) is the concentration of Pb(II) in the solution at time t.

The pseudo-first-order (Eq. (3)) and pseudo-second-order (Eq. (4)) kinetic models are commonly used to test experimental data [13, 41–47].

$$q_t = q_1 \times \left(1 - e^{-k_1 \times t}\right),$$ (3)

$$q_t = \frac{q_2^2 \times k_2 \times t}{(1 + q_2 \times k_2 \times t)},$$ (4)

where k_1 (min^{-1}) and k_2 (g mg^{-1} min^{-1}) and q_1 and q_2 (mg g^{-1}) are the rate constants and the maximum adsorption capacities of the pseudo-first-order and pseudo-second-order adsorption kinetic models, respectively.

2.5.3. Effect of Solution pH. Mn/diatomite (0.02 g) was placed into an Erlenmeyer flask containing 50 mL of the Pb(II) solution with a specified concentration and pH (the pH value of the solution was adjusted with a 0.1 M HCl or 0.1 M NaOH solution) and shaken at ambient temperature for 3 h to achieve adsorption-desorption equilibrium. Then, the adsorbent was removed, and the Pb(II) concentration was determined.

2.5.4. Equilibrium Studies. In this section, the adsorption was performed at 303 K, and the initial concentration of Pb(II) varied between 30.8 and 188.3 mg L^{-1} ($V = 0.1$ L; $m = 0.1$ g). To analyze the data of Pb(II) adsorption onto Mn/diatomite, we used the Freundlich, Langmuir and Sips models.

The Freundlich model assumes heterogeneous energy distribution of the active sites on the adsorbent surface with the interactions within the adsorbate. The Freundlich isotherm can be expressed in the following equation [13, 37, 41, 42, 45–47].

$$q_e = K_F \times C_e^{1/n},$$ (5)

where K_F is the Freundlich constant (mg$^{(1-1/n)}$ L$^{1/n}$ g^{-1}) and n is the adsorption intensity. Theoretically, the adsorption conditions are favourable if the n constant is greater than 1.

The Langmuir isotherm is a theoretical model for monolayer adsorption to a surface containing a finite number of adsorption sites with uniform adsorption energies without the displacement of the adsorbate in the plane of the adsorbent surface. The Langmuir isotherm is expressed in the following equation [10, 11, 37, 41–43, 45–47].

$$q_e = \frac{q_m \times K_L \times C_e}{1 + K_L \times C_e},$$ (6)

where the K_L constant is related to the adsorption energy (L g^{-1}) and q_m is the Langmuir monolayer adsorption capacity (mg g^{-1}).

The Sips isotherm has a form similar to the Freundlich isotherm, but it has a finite limit when the concentration is sufficiently high. The Sips equation can be expressed in the following equation [48].

$$q_e = \frac{q_{m_S} \times K_S \times C_e^{m_S}}{1 + K_S \times C_e^{m_S}}, \tag{7}$$

where the K_S ($L^m\,mg^{m-1}$) and q_{m_S} ($mg\,g^{-1}$) are the Sips equilibrium constant and maximum adsorption capacity, respectively, and m_S is the Sips model exponent.

Isothermal and kinetic parameters were determined from nonlinear regression with the Solver tool in Microsoft Excel [49–51] with the root-mean-square error (RMSE) function described in the following equation [49, 50].

$$RMSE = \sqrt{\frac{1}{N}\sum_{i=1}^{N}\left(q_{e,exp} - q_{e,cal}\right)_i^2}, \tag{8}$$

where $q_{e,exp}$ and $q_{e,cal}$ are the adsorption capacity values obtained from the experiment and models, respectively, and N represents the number of data points.

2.5.5. Thermodynamic Studies. In this section, the initial concentration of Pb(II) was kept constant ($V = 0.1\,L$, $m = 0.1\,g$, $C_0 = 75\,mg\,L^{-1}$). The adsorption was performed at temperatures ranging from 303 to 338 K. The feasibility of the adsorption process can be estimated through thermodynamic studies. The thermodynamic parameters of Pb(II) adsorption on Mn/diatomite were calculated using the following equations [15, 37].

$$K_C = \frac{C_0 - C_e}{C_e} \times \frac{V}{m} = \frac{q_e}{C_e}, \tag{9}$$

$$\ln K_C = -\frac{\Delta H^\circ}{R \times T} + \frac{\Delta S^\circ}{R}, \tag{10}$$

where R ($8.314\,J\,mol^{-1}\,K^{-1}$) is the ideal gas constant and T (K) is the absolute temperature. ΔH° is the enthalpy change, and ΔS° is the entropy change of the adsorption process.

The free energy change ΔG° of the adsorption process is calculated according to the following equation [15, 37].

$$\Delta G^\circ = \Delta H^\circ - T \times \Delta S^\circ. \tag{11}$$

The adsorption rate constant (k) of the adsorption process is a temperature-dependent function expressed in the following Arrhenius equation [41, 46].

$$\ln k = \ln A - \frac{E_a}{R \times T}, \tag{12}$$

where E_a is the Arrhenius activation energy ($J\,mol^{-1}$) and A is the Arrhenius constant.

2.5.6. Desorption Experiments. After each experiment, the adsorbent was recycled. The desorption was performed by mixing the used adsorbent with 0.1 M HCl solution (a ratio of 0.5 g/50 mL). The mixture was then shaken with a shaker at ambient temperature ($29 \pm 2°C$) at 200 rpm for 120 min, filtered to recover the adsorbent, and washed with distilled water for subsequent readsorption.

3. Results and Discussion

3.1. Modification of Diatomite with Manganese Oxide and Pb(II) Adsorption Capacity Assessment

3.1.1. Effect of Hydrothermal Temperature. The morphology of natural diatomite and the Mn/diatomite samples prepared at different hydrothermal temperatures is presented in Figure 1. Natural diatomite exists as cylindrical tubes with a 5-7 μm diameter. Its surface is relatively smooth and has pores with a diameter of about 0.5 μm (Figure 1(a)). The morphology of manganese oxide varies from a flower-like structure to a needle-like one with an increase in the hydrothermal temperature. The Mn/diatomite sample prepared at 80°C exhibits flower-like particles attached to the diatomite surface and pores (Figure 1(b)). The morphology of the flower-like particle with some hundred nanometers in diameter consists of thin plates embroiled together. At the hydrothermal temperatures of 120 and 160°C, needle-like manganese oxide appears and is dispersed on the surface and in the pores of natural diatomite (Figures 1(c) and 1(d)).

Natural diatomite has a moderate adsorption capacity ($15.6\,mg\,g^{-1}$) compared with Mn/diatomite ($26.3-32.9\,mg\,g^{-1}$). Although all samples have a higher adsorption capacity, the one prepared at 80°C outweighs the others ($32.9\,mg\,g^{-1}$) despite its lowest manganese content (Table S1). Thus, it can be assumed that manganese does not support Pb(II) adsorption. Instead, the material structure may favour adsorption because the denaturation at 80°C forms a material with a flower-like configuration. Therefore, this temperature was chosen for further experiments.

3.1.2. Effect of Molar Ratio of Precursors. The molar ratio between $KMnO_4$ and HCl was chosen at 1:1, 1:2, and 1:4. At the ratio of 1:1 (Figures 2(a) and 2(b)), the sample has a large number of circular or rod-shaped clusters attached to the surface of diatomite. At the ratio of 1:2 (Figures 2(c) and 2(d)), the circular clusters become larger, and spheres with a flower-like membrane structure appear (like the Mn/diatomite sample prepared at the molar ratio of $KMnO_4$/HCl 1:8; Figure 1(b)). Finally, at the ratio of 1:4 (Figures 2(e) and 2(f)), besides the spheres with the flower-like membrane structure, film-like structures are formed uniformly on the surface of the diatomite, thus increasing the Pb(II) adsorption efficiency. In this case, the structure of Mn-modified diatomite decides the Pb(II) adsorption efficiency, and the ratio of 1:4 provides the highest efficiency ($43.1\,mg\,g^{-1}$, Table S1). Therefore, this ratio was chosen for subsequent experiments.

3.1.3. Effect of Hydrothermal Time. In this section, we investigate the hydrothermal time under the conditions found above (Figure 3). The figure shows the SEM images of the 24 and 48 h samples with flower-like spheres and a regular layer of membranous structures. This topography is similar to that of the 16 h samples (Figures 2(e) and 2(f)). Concerning the content of manganese, it seems that a longer hydrothermal time favours the amount of this element in the sample and thus, together with the membranous structures, enhances Pb(II) adsorption (Table S1). From these results,
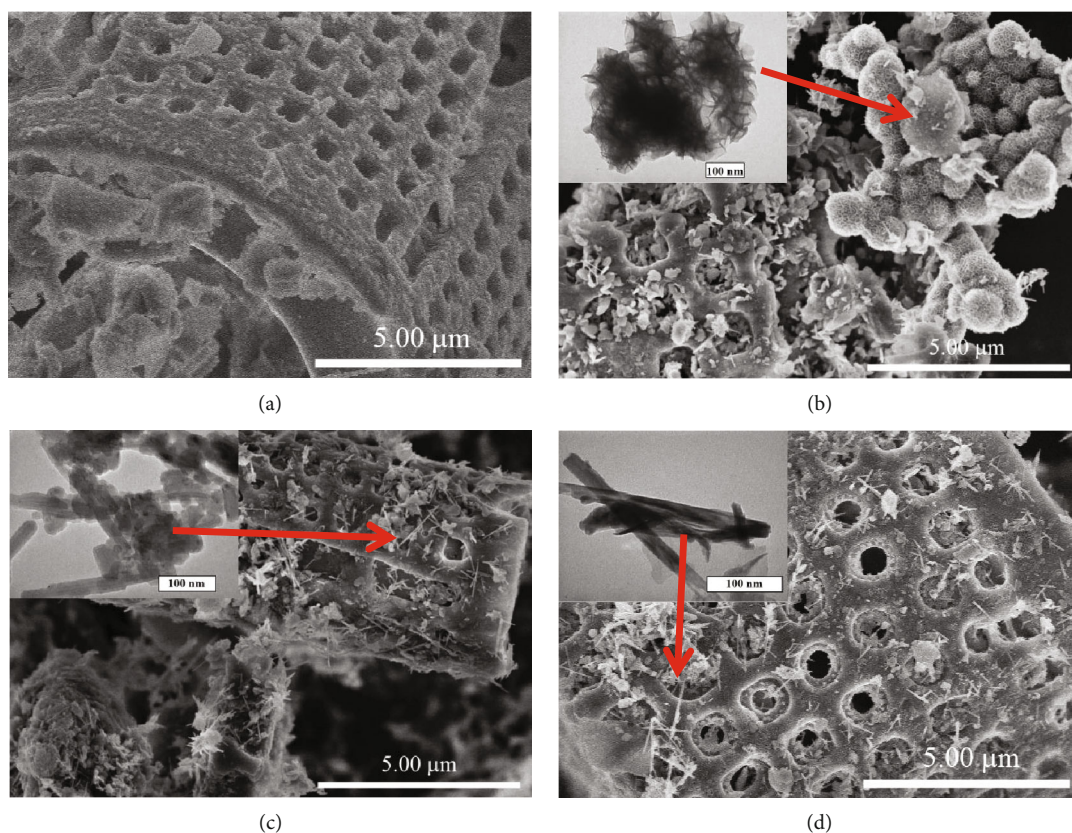
FIGURE 1: SEM images of diatomite (a) and the Mn/diatomite samples prepared at different hydrothermal temperatures: (b) 80°C; (c) 120°C; (d) 160°C, and the insets present TEM images (experimental conditions: hydrothermal time of 16 h and molar ratio of KMnO$_4$/HCl 1 : 8).

we choose 24 h (54 mg g^{-1} Pb(II) adsorption efficiency) as the appropriate time for further studies. The 24 h sample was denoted as Mn/diatomite and used for characterization.

The crystalline phase of natural diatomite and the Mn/diatomite was analyzed based on the X-ray data. For natural diatomite, the XRD pattern displays characteristic diffraction peaks of amorphous silica (broad diffraction centered at 20-25°) [52–56]. As for Mn/diatomite samples prepared at different hydrothermal temperatures, no characteristic diffraction peaks of manganese oxide are observed (Figure 4(a)), which is probably because manganese oxide particles are very small and evenly distributed on the surface of diatomite or because diatomite hinders the X-ray diffraction of manganese oxide. This result is consistent with that reported by Li et al. [36].

The XRD pattern of Mn/diatomite (Figure 4(b)) shows characteristic diffraction peaks of amorphous silica at 20–25° [52–56] and the peaks for MnO$_2$ (JCPDS No. 00-024-0735) with low intensity because of the oxide's small size and its uniform distribution on the surface of diatomite, as mentioned above.

The textural properties of natural diatomite and Mn/diatomite indicate the type II isotherm and a H3-type hysteresis loop (Figure 4(c)), corresponding to the existence of macropores of nonuniform size and/or shape [57]. Besides, the Mn/diatomite sample with significant condensation at high relative pressures ($P/P \circ \sim \mathbf{1}$) indicates the existence of a slit-pore structure because the pores formed between membrane of the modified material.

The pore-size distribution curve (Figure 4(d)) indicates that natural diatomite has pores of about 4.3 nm in diameter, while the Mn/diatomite sample has smaller pores (3.9 nm). This decrease is caused by the manganese oxide film coated on the surface. However, the specific surface area of Mn/diatomite ($S_{BET} = 68.5$ m^2 g^{-1}) is larger than that of natural diatomite ($S_{BET} = 55.4$ m^2 g^{-1}) (Table S2) because of the space formed between the sheets of manganese oxide attached to the diatomite surface. However, this specific area difference is insignificant.

3.2. Characteristic Properties and Pb(II) Adsorption Capacity of Nano-MnO$_2$. Nano-MnO$_2$ was prepared from KMnO$_4$ and HCl with four molar ratios of 1 : 1, 1 : 2, 1 : 4, and 1 : 8. All the samples have a bar shape with sides of about 60 to 100 nm (Figure 5), very similar to what was prepared by Wu et al. [40]. Some bars have a hollow tip like a tube. Except for the 1 : 1 KMnO$_4$/HCl sample, which has the bars stacked together, the other three samples have more or less separate bars with an insignificant number of stacks.

The MnO$_2$ samples have the crystalline structure of an α-MnO$_2$ crystal with characteristic XRD peaks at 28.8, 37.6, 42.1, 49.8, 56.0, and 60.2° (Figure 6), corresponding to the (310), (211), (301), (411), (600), and (521) planes (JCPDS No. 00-024-0735) [40, 58, 59]. The sharp peaks with high intensity of the 1 : 2 to 1 : 8 KMnO$_4$/HCl samples indicate that the formed α-MnO$_2$ has high crystallinity and
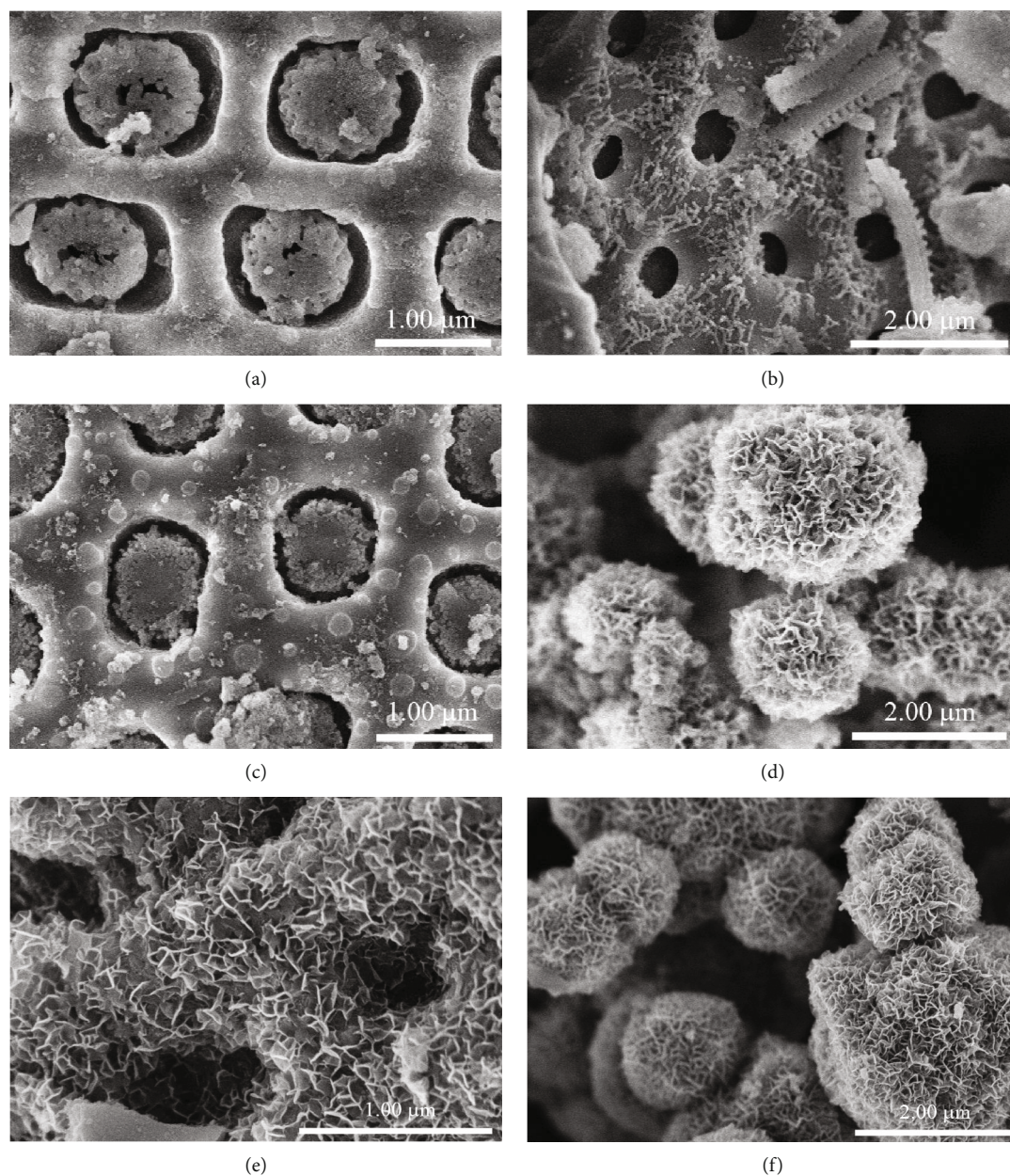
(a)

(b)

(c)

(d)

(e)

(f)

FIGURE 2: SEM images of Mn/diatomite samples prepared at different KMnO$_4$/HCl molar ratios: (a, b) 1:1; (c, d) 1:2; (e, f) 1:4 (experimental conditions: hydrothermal time and temperature are 16 h and 80°C, respectively).

order. The sample at the KMnO$_4$/HCl 1:1 ratio has sharp peaks with low intensity, showing a low-ordered material. This observation is completely consistent with the results observed with SEM in Figure 5(a).

The nano-MnO$_2$ samples were subjected to Pb(II) adsorption in the aqueous solution. Their adsorption capacities are similar with low values (16.2-18.9 mg g^{-1} at $C_{0,Pb(II)} = 70.6$ mg L^{-1}) (Figure S1). However, the Pb atoms are uniformly distributed over the entire area of the MnO$_2$ nanomaterial (Figure S2). The distribution of elements on the Mn/diatomite samples before Pb(II) adsorption shows that the material contains primarily Si and O with some Fe, Al, and Mn (Figure S3). After adsorption, the mapping

displays Pb besides other elements. Manganese and Pb are uniformly distributed throughout the material surface, indicating that Pb adsorbs onto the Mn/diatomite material (Figure S4).

The FT-IR spectra of natural diatomite, Mn/diatomite, and Mn/diatomite after Pb(II) adsorption are relatively similar (Figure 7(a)), with a broad band at 1100 cm^{-1} and two narrow bands at 797 and 470 cm^{-1}, corresponding to the asymmetric and symmetric stretching vibrations and bending vibration of the Si-O-Si bonds, respectively [13, 19, 55]. The peaks at 3697 and 3621 cm^{-1} are typical for surface hydroxyl groups in diatomite, with the former corresponding to the isolated hydroxyl group (Si-OH) on the surface
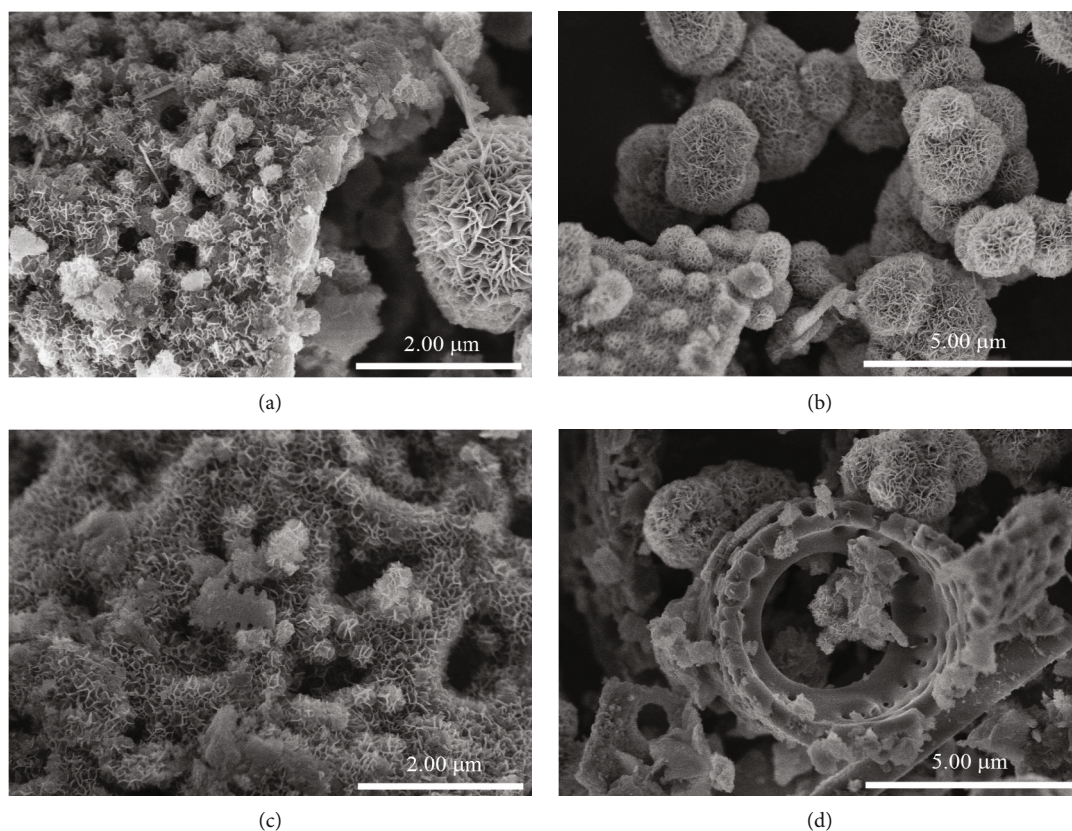
FIGURE 3: SEM images of Mn/diatomite samples prepared at different hydrothermal times: (a, b) 24 h; (c, d) 48 h (experimental conditions: hydrothermal temperature of 80°C and molar ratio of $KMnO_4$/HCl 1:4).

of diatomite [55, 60, 61], and the latter due to O-H stretching vibration of the aluminol groups (≡AlOH) [61]. These bands of Mn/diatomite have a lower intensity, indicating the chemical interaction between the surface silanol groups and the oxides [13]. The broad bands at 3441 and $1637 \, cm^{-1}$ are thought to be due to the vibrations of the O-H bonds of adsorbed H_2O molecules, including free adsorbed water and hydrogen-bonded water with surface hydroxyl groups. The absorption band at $533 \, cm^{-1}$ is thought to be the stretching vibration of the Fe-O bond [55] or the Me-O bond (with Me being a metal). The bands observed at 431-435 and $419\text{-}426 \, cm^{-1}$ in Mn/diatomite and nano-MnO_2 (Figure 7(b)) are probably another vibration characteristic for Mn-O binding (not present in the diatomite sample). For the Mn/diatomite sample after Pb(II) adsorption, the intensity of the absorption bands is very low, probably because of the adsorbed Pb(II) layer. In particular, no vibrations are observed at wavenumbers lower than $470 \, cm^{-1}$. This is probably because the Pb(II) ions are bound to the manganese oxide adsorption sites.

3.3. Adsorption of Pb(II) on Mn/Diatomite

3.3.1. Adsorption Kinetics of Pb(II) on Mn/Diatomite. Chemical kinetics is indispensable in adsorption studies to determine the adsorption rate of the adsorbate at the solid interface. Kinetic models allow the estimation of adsorption rates and lead to suitable rate expressions and suggestion of possible reaction mechanisms.

We can see that the adsorption efficiency of Pb(II) increases with an increase in contact time and initial concentration (Figure 8). This increase probably depends on the concentration difference of Pb(II) ions on the adsorbent surface and in the solution (driving force). When the initial concentration is small, the driving force is also small, leading to a low adsorption efficiency. The adsorption efficiency increases with the driving force, but this increase becomes smaller when the initial concentration is higher. Figure 8 also shows that the Pb(II) adsorption occurs very rapidly during the first 10 min of contact; then, it decreases slowly in the next 60 min and becomes stable after 240 min. Thus, the time required for the adsorption of Pb(II) on Mn/diatomite to reach the adsorption-desorption equilibrium is 60 min.

The adsorption kinetics were described by using the pseudo-first/second-order kinetic models, and the results are presented in Tables 2 and 3. It was found that the equilibrium adsorption capacity values, q_2, calculated from the pseudo-second-order equation, are very close to the experimental equilibrium adsorption capacity values, q_e. The kinetic data fit the pseudo-second-order kinetic model better than the pseudo-first-order kinetic model because the former's RMSE values are smaller, and the data points are closer to the theoretical line than the latter's (Figure S5). Since the pseudo-second-order kinetic model is derived
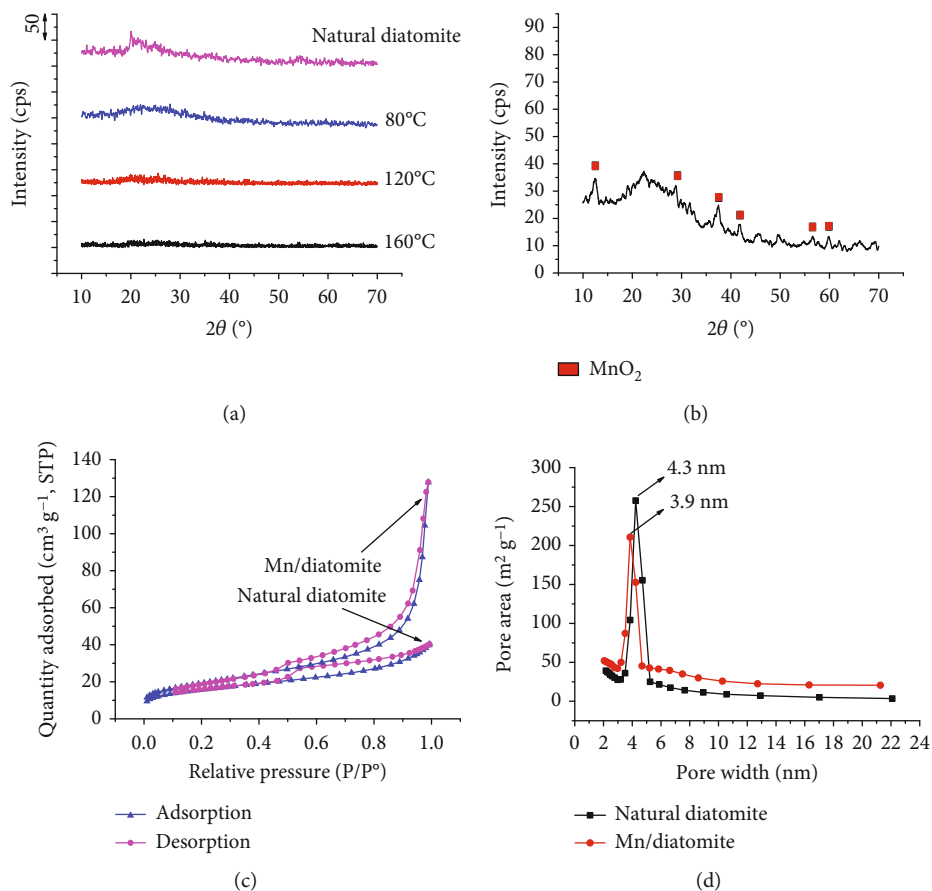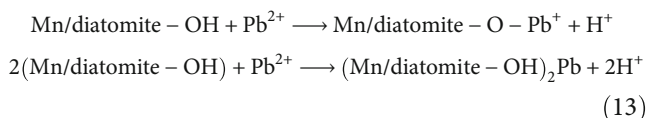
(a)

■ MnO$_2$

(b)

(c)

(d)

FIGURE 4: (a) XRD patterns of natural diatomite and the Mn/diatomite samples prepared at different hydrothermal temperatures (experimental conditions: hydrothermal time of 16 h and molar ratio of KMnO$_4$/HCl 1 : 8); (b) XRD pattern of the Mn/diatomite sample (experimental conditions: hydrothermal time and temperature of 24 h and 80°C, respectively, and molar ratio of KMnO$_4$/HCl 1 : 4); (c) nitrogen adsorption-desorption isotherms; (d) pore-size distributions of diatomite and Mn/diatomite (experimental conditions: hydrothermal time and temperature of 24 h and 80°C, respectively, and molar ratio of KMnO$_4$/HCl 1 : 4).

from the assumption that the rate-limiting step is chemical adsorption, it is concluded that the adsorption process is controlled by chemisorption.

3.3.2. Effect of Solution pH. Figure 9(a) displays the pH effect on the Pb adsorption efficiency. Overall, it is clear that the adsorption efficiency increases consistently with increasing pH. The adsorption efficiency soars from pH 2 to pH 5 and then increases steadily up to pH 6. The Pb(II) species can be in the forms of Pb^{2+}, Pb(OH)$^+$, Pb$_3$(OH)$_4$$^{2+}$, Pb(OH)$_2$, and Pb(OH)$_3$$^-$, depending on the solution pH [62]. The cation form Pb^{2+} mainly exists at pH < 5, while hydroxyl anions of lead are predominant at pH > 5. The increasing adsorption at low pH (<pH$_{PZC}$, Figure 9(b)) is explained by the fact that the adsorbent surface becomes less positively charged with increasing pH, enhancing the electrostatic interaction between the adsorbate and the surface. At higher pH (>pH$_{PZC}$), the adsorption capacity increases slightly because of the electrostatic repulsion of the more negative adsorbate and the negatively charged surface. This fact also indicates that the electrostatic interaction is not the only mechanism of the adsorption process. The pH$_{PZC}$ of Mn/diatomite after Pb adsorption shifts to low pHs, indicating that the high

adsorption efficiency of Mn/diatomite under weak acidic/ alkaline conditions could be attributed to the formation of complexes between Pb(II) and the surface hydroxyl groups of the Mn/diatomite. The formation of outer-sphere surface complexes could not shift the point of zero charge of the absorbent because there are no specific chemical reactions among the lead cations that could change the surface charge. The shift of the point of zero charge to a lower pH range indicates the formation of anionic negatively charged surface complexes [63]. Hence, the decrease in pH$_{PZC}$ to 3.2 implies that the adsorption of lead would be a result of the formation of both outer-sphere complexes and the negatively charged inner-sphere complexes between lead and the adsorbent. Then, the possible adsorption reaction of Mn/diatomite with Pb(II) can be shown schematically as follows:

At low pH, Pb(II) reacts with hydroxyl groups (silanol, Mn-OH) on the surface of Mn/diatomite to form complex adsorption:
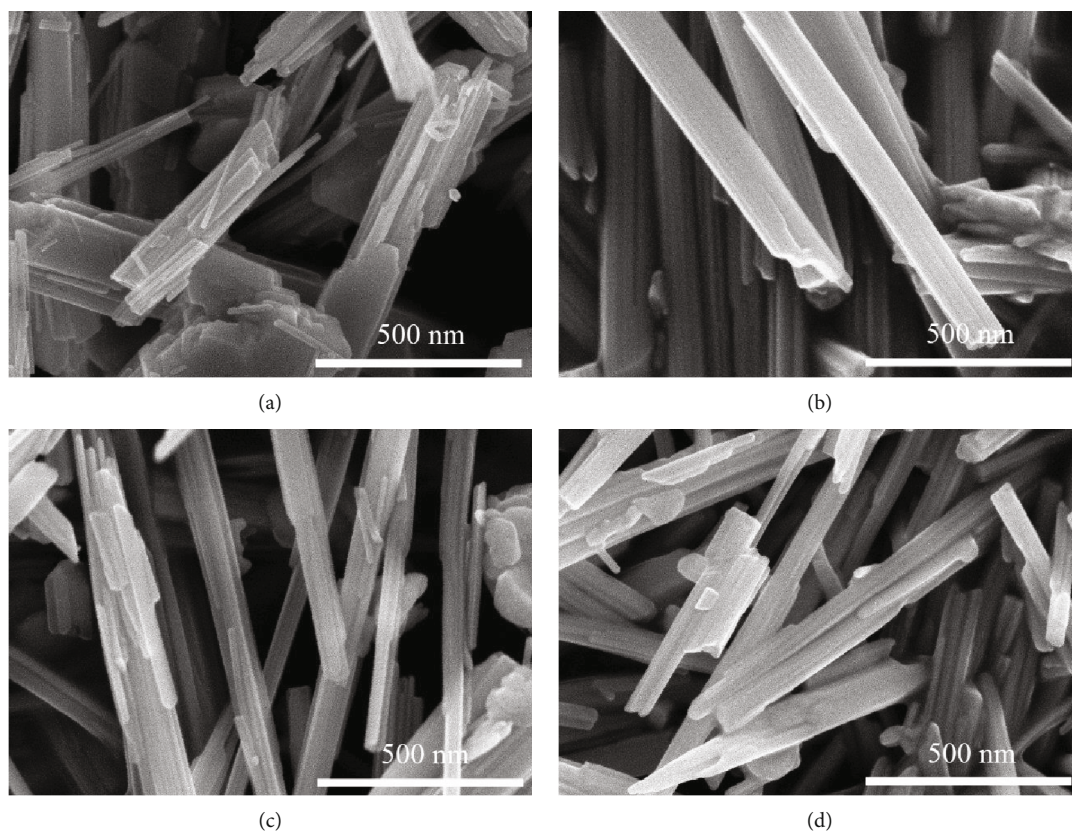
$$Mn/diatomite - OH + Pb^{2+} \longrightarrow Mn/diatomite - O - Pb^+ + H^+$$

$$2(Mn/diatomite - OH) + Pb^{2+} \longrightarrow (Mn/diatomite - OH)_2 Pb + 2H^+$$

(13)

FIGURE 5: SEM images of MnO_2 samples synthesized at different molar ratios of $KMnO_4$/HCl: (a) 1:1; (b) 1:2; (c) 1:4; (d) 1:8 (experimental conditions: hydrothermal time and temperature are 16 h and 160°C, respectively).
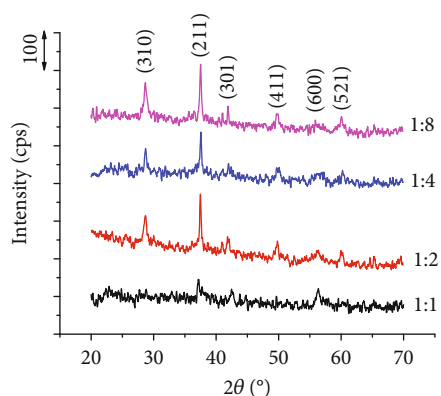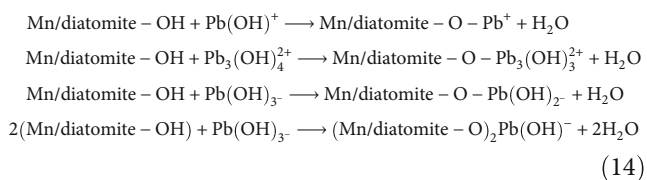

FIGURE 6: XRD pattern of MnO_2 samples synthesized at different $KMnO_4$/HCl molar ratios (experimental conditions: hydrothermal time and temperature are 16 h and 160°C, respectively).

At high pH, hydroxyl anions of lead react with hydroxyl groups (silanol, Mn-OH) on the surface of Mn/diatomite to form complex adsorption:

$$Mn/diatomite - OH + Pb(OH)^+ \longrightarrow Mn/diatomite - O - Pb^+ + H_2O$$

$$Mn/diatomite - OH + Pb_3(OH)_4^{2+} \longrightarrow Mn/diatomite - O - Pb_3(OH)_3^{2+} + H_2O$$

$$Mn/diatomite - OH + Pb(OH)_3^- \longrightarrow Mn/diatomite - O - Pb(OH)_2^- + H_2O$$

$$2(Mn/diatomite - OH) + Pb(OH)_3^- \longrightarrow (Mn/diatomite - O)_2 Pb(OH)^- + 2H_2O$$

$$(14)$$

3.3.3. Adsorption Isotherms.

The study of adsorption isotherms is essential in describing the characteristic relationship between the concentration of the adsorbate and the adsorption capacity of the adsorbent, especially when designing an ideal adsorption system in industry [42, 45].

The results of the determination of isotherm parameters of Pb(II) adsorption on Mn/diatomite, natural diatomite, and nano-MnO_2 are presented in Table 4 (and Figure S6). Based on the RMSE value, it can be assumed that the Freundlich and Sips models are more suitable to describe the adsorption of Mn/diatomite and natural diatomite than the Langmuir model. On the contrary, the Sips and Langmuir models are more suitable than the Freundlich model to describe the adsorption on nano-MnO_2. To evaluate the compatibility of models with experimental data, numerous authors have used statistical methods, such as the paired-sample t-test [49], Akaike's information criteria (AIC) [51], and the sum of normalized errors (SNE) [50]. In general, these methods are based on the relationship between the experimental and calculated adsorption capacities. Figure 10(a) depicts the Langmuir, Freundlich, and Sips isotherms for Pb(II) adsorption on Mn/diatomite. The complete fit occurs when the points lie on the diagonal ($x = y$). It can be seen that the Freundlich and Sips models have a lower dispersion; that is, there are smaller gaps between the prediction of these models and the experimental data. However, the Sips maximum adsorption capacity values (q_{m_S}) for Mn/diatomite and
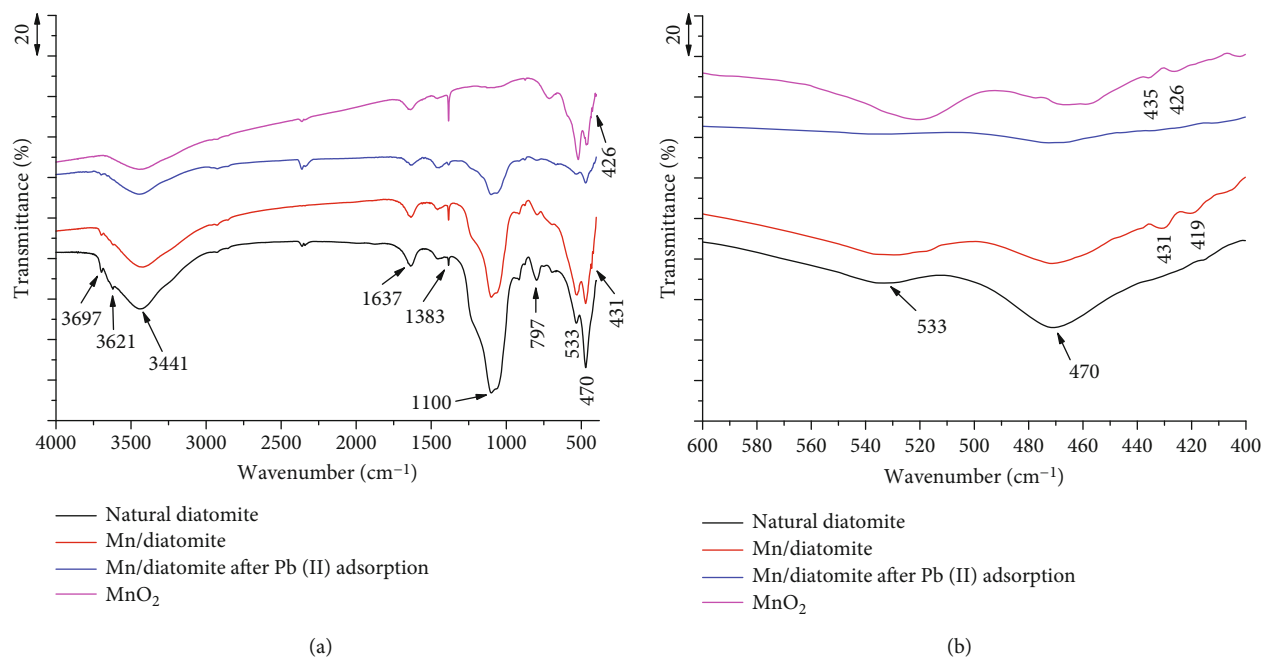
(a)

(b)

FIGURE 7: FT-IR spectra of natural diatomite, Mn/diatomite, Mn/diatomite after Pb(II) adsorption, and MnO$_2$: (a) wavenumber region 4000-400 cm^{-1}; (b) wavenumber region 600-400 cm^{-1}.
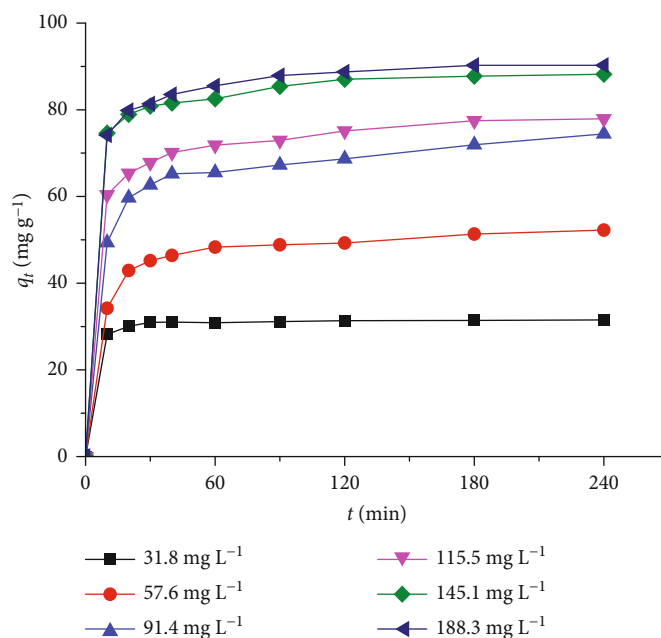

FIGURE 8: Adsorption kinetics of Pb(II) onto Mn/diatomite with the different initial concentrations ($V = 0.1$ L; m of adsorbent $= 0.1$ g; temperature: 303 K; pH$_{initial} = 6.19 \div 5.12$; pH$_{final} = 6.00 \div 4.53$).

natural diatomite are much larger than the experimental equilibrium adsorption capacity values (see Tables 2 and 3 and Table S1), indicating that the Sips model does not sufficiently satisfy describing these adsorption processes. Meanwhile, the maximum adsorption capacity values obtained from the Langmuir and Sips equations of nano-MnO$_2$ are approximately the same, indicating the similarity between these two models.

The maximum capacity of monolayer adsorption determined with the nonlinear Langmuir model is $81.42 \, \text{mg g}^{-1}$. Our value is slightly smaller than that published by Khraished et al. [11] ($99.00 \, \text{mg g}^{-1}$) but higher than Li et al.'s value ($56.843 \, \text{mg g}^{-1}$) [36] and other authors' values (Table 5). The maximum adsorption capacity of natural diatomite and nano-MnO$_2$ is 16.31 and $19.42 \, \text{mg g}^{-1}$, respectively. These values are significantly smaller than the maximum adsorption

TABLE 2: Kinetic parameters of Pb(II) adsorption on Mn/diatomite at different initial concentrations of Pb(II) solutions.

Initial Pb(II) concentration (mg L^{-1})	q_e (mg g^{-1})	Pseudo-first-order			Pseudo-second-order		
		k_1 (min^{-1})	q_1 (mg g^{-1})	RMSE	k_2 (g mg^{-1} min^{-1})	q_2 (mg g^{-1})	RMSE
31.8	31.5	0.2321	31.1	0.334	0.0272	31.7	0.208
57.6	52.2	0.1085	49.2	1.724	0.0038	52.4	0.689
91.4	74.4	0.1149	68.4	3.113	0.0029	72.8	1.497
115.5	77.9	0.1561	73.1	3.408	0.0041	76.8	1.500
145.1	88.2	0.2037	84.4	2.877	0.0059	87.3	1.373
188.3	90.3	0.1809	86.5	3.150	0.0046	90.0	1.211

TABLE 3: Pb(II) adsorption kinetic parameters on Mn/diatomite at different adsorption temperatures.

Temperature (K)	q_e (mg g^{-1})	Pseudo-first-order			Pseudo-second-order		
		k_1 (min^{-1})	q_1 (mg g^{-1})	RMSE	k_2 (g mg^{-1} min^{-1})	q_2 (mg g^{-1})	RMSE
303	52.4	0.1347	49.8	2.003	0.0052	52.4	0.577
313	61.8	0.1461	58.9	2.810	0.0047	62.1	1.112
323	67.5	0.3386	66.0	0.860	0.0283	66.7	0.517
328	71.8	0.2527	69.7	1.678	0.0115	71.4	0.777
333	74.5	0.3319	72.6	1.412	0.0200	73.7	0.907
338	74.8	0.3345	73.3	0.994	0.0237	74.2	0.536
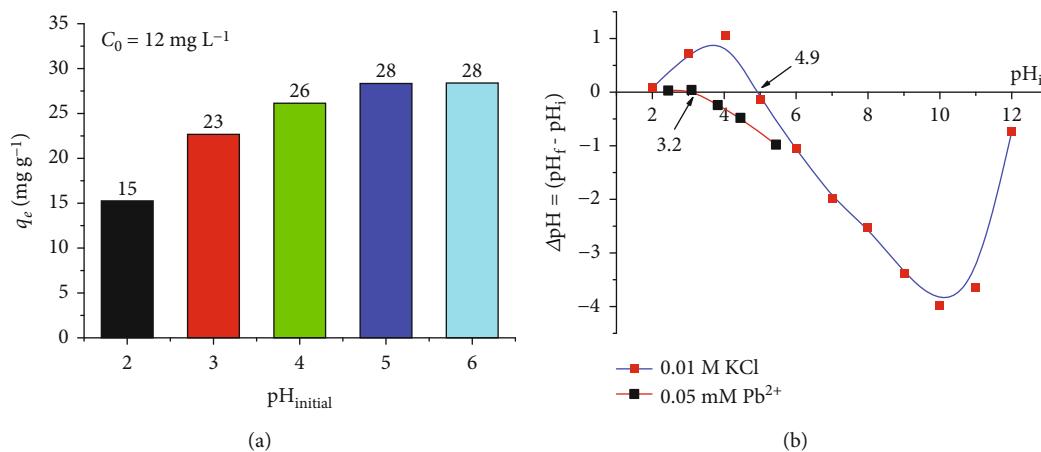
FIGURE 9: (a) Pb(II) adsorption capacity on Mn/diatomite at different solution pHs; (b) point of zero charge of Mn/diatomite in 0.01 M KCl solution and in 0.05 mM Pb^{2+} solution determined by the pH drift method [64].

capacity of Mn/diatomite. Because a layer of manganese oxide coats the diatomite, this material has an increased adsorption capacity, indicating that Mn/diatomite is not merely a physical mixture of natural diatomite and nano-MnO$_2$ but is a composite with a high adsorption capacity.

3.3.4. Adsorption Thermodynamics. We can see that the adsorption capacity depends on the temperature in a similar manner to that of the initial concentration (Figure 10(b)). At lower temperatures (303–323 K), the maximal capacity increases more rapidly than at higher temperatures (323–338 K), and it remains practically the same at 333 and 338 K. This behaviour is also revealed from the slope of the lines during the first 10 min of adsorption. The higher the

temperature, the steeper the line is. For all the temperatures, the adsorption-desorption equilibrium is reached after around 60 min.

The plot of ln K_C against $1/T$ is shown in Figure 11(a). From the intercept and slope of the regression line, we calculate $\Delta H°$ and $\Delta S°$ from Eq. (10) and $\Delta G°$ from Eq. (11) (Table 6). Figure 11(a) shows that Pb(II) adsorption on Mn/diatomite is strongly dependent on temperature. The temperature range from 303 to 338 K can be divided into two ranges: range 1 from 303 to 323 K and range 2 from 323 to 338 K. In both temperature ranges, $\Delta H° > 0$, indicating that the adsorption is endothermic; that is, as the temperature increases, the adsorption capacity increases. This result is entirely consistent with the adsorption data shown

TABLE 4: Parameters of the nonlinear models for the adsorption of Pb(II) in an aqueous solution on Mn/diatomite, natural diatomite, and nano-MnO$_2$.

Isotherm model	Parameter	Adsorbent		
		Mn/diatomite	Natural diatomite	Nano-MnO$_2$
Langmuir (2p)*	K_L (L g^{-1})	1.18	4.98	7.54
	q_m (mg g^{-1})	81.42	16.31	19.42
	RMSE	10.17	1.63	0.73
Freundlich (2p)*	K_F (mg$^{(1-1/n)}$ L$^{1/n}$ g^{-1})	41.09	11.20	15.43
	n	5.54	5.95	10.35
	RMSE	3.46	0.49	1.45
Sips (3p)*	K_S (L^m mg^{m-1})	0.27	0.05	18.49
	q_{m_S} (mg g^{-1})	188.74	240.09	18.93
	m_S	0.28	0.18	1.58
	RMSE	3.10	0.50	0.62

*Number of parameters.
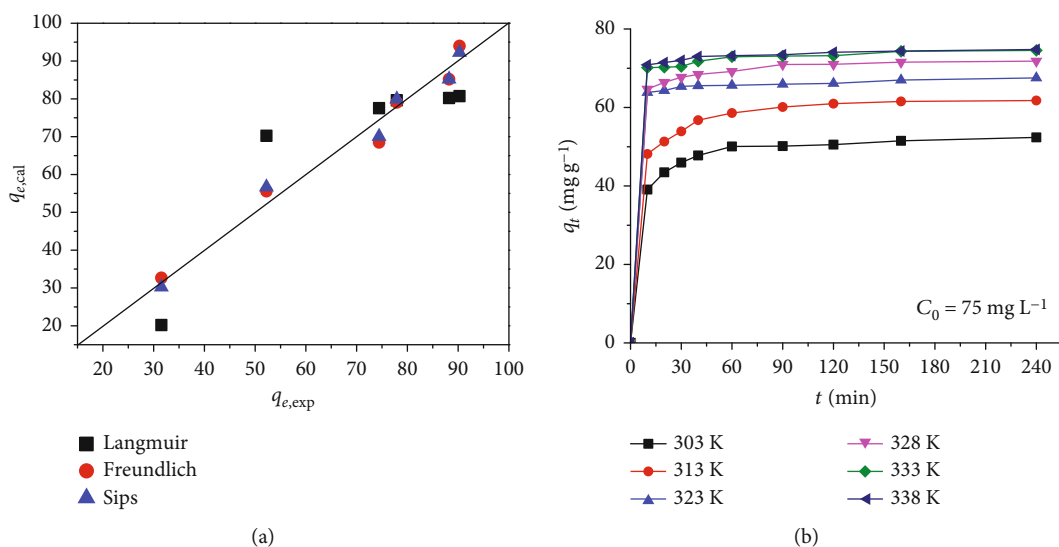
FIGURE 10: (a) Relationship between the experimental and the calculated adsorbed amount for the adsorption of Pb(II) on Mn/diatomite; (b) effect of temperature and contact time on the adsorption capacity of Pb(II) in aqueous solution of Mn/diatomite (pH$_{initial}$ = 5.48).

in Figure 10(b). Furthermore, range 2 has a much larger $\Delta H°$ (234.222 kJ mol^{-1}) than range 1, in which $\Delta H° = 55.451$ kJ mol^{-1}. This suggests that the adsorption process occurs favourably at high temperatures, suggesting chemical adsorption onto the composite.

The negative value of $\Delta G°$ in the 303–338 K range shows that the Pb(II) adsorption in aqueous solutions on Mn/diatomite is spontaneous. Meanwhile, the positive $\Delta S°$ reflects the increase in the degree of free movement at the solid/solution interface in the adsorption process [13, 43, 44, 46].

Since the Pb(II) adsorption on Mn/diatomite follows the pseudo-second-order kinetic model, the adsorption rate constant k_2 is used in Eq. (12). Figure S7 depicts the plot of $\ln(k_2)$ versus $1/T$, and the activation energy of Pb(II) adsorption in aqueous solutions on Mn/diatomite material is 41.56 kJ mol^{-1}. Usually, physisorption has an activation energy in the range of 5-40 kJ mol^{-1}, while that of chemisorption is generally in the range of 40-800 kJ mol^{-1} [46]. Therefore, the adsorption of Pb(II) on Mn/diatomite could occur via the formation of weak chemical bonds between the adsorbent and the adsorbate [41].

3.3.5. Recycling Studies.

The regeneration of the spent Mn/diatomite adsorbent was carried out in three adsorption-desorption cycles. The readsorption experiments were performed on 50 mL of Pb(II) solution with pH and initial concentration of 5.45 and 80.1 mg L^{-1}, respectively, and 0.05 g of the adsorbent. The mixture was shaken with a shaker at 200 rpm for 3 h at ambient temperature (29 ± 2°C). Then, the adsorbent was removed by filtration, the remaining Pb(II) concentration was determined, and the adsorption capacity was calculated. The results show

TABLE 5: Pb(II) adsorption capacity of different adsorbents.

| Adsorbent	Adsorption capacity (mg g^{-1})	pH	Reference
Mn/diatomite	81.42 (303 K)	Neutral	This work
Natural diatomite	16.31 (303 K)	Neutral	This work
Nano-MnO$_2$	19.42 (303 K)	Neutral	This work
Mn/diatomite	99 (289 K)	4	[10]
Diatomite	24.94 (296 K)	4	[11]
Mn/diatomite	99 (296 K)	4	[11]
Raw DE	8.5058 (303 K)	Neutral	[36]
MnO$_2$@DE	56.843 (303 K)	Neutral	[36]
Silicalite-1-NH$_2$	43.5 (298 K)	5.5	[65]
MCM-48-NH$_2$	75.2 (298 K)	5.5	[65]
MCM-48-SH	31.2 (298 K)	5.5	[65]
Aminopropyl-MCM-41	64.21 (300 K)	Neutral	[49]
Leonardite	23.89 (303 K)	6	[50]
Biological sludge through ferric activation	42.96 (298 K)	5	[7]
Chitosan-tripolyphosphate bead	57.33 (300 K)	4.5	[44]
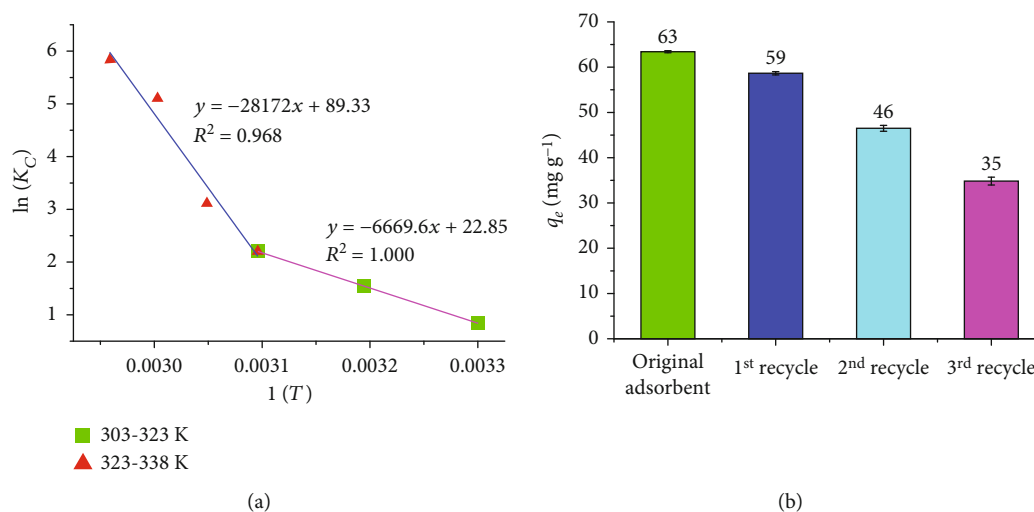
FIGURE 11: (a) Linear plot of ln (K_C) versus $1/T$ and (b) Pb(II) adsorption capacity in aqueous solution of reused Mn/diatomite samples (experimental conditions: 0.05 g of the adsorbent and 50 mL of Pb(II) solution with $C_0 = 80.1$ mg L^{-1}; each experiment was repeated three times).

TABLE 6: Thermodynamic parameters of Pb(II) adsorption on Mn/diatomite.

T (K)	ΔG^o (kJ mol^{-1})	ΔH^o (kJ mol^{-1})	ΔS^o (J mol^{-1} K^{-1})
303	-2.111	55.451	189.975
313	-4.011		
323	-5.911		
323	-5.667	234.222	742.690
328	-9.380		
333	-13.094		
338	-16.807		

that the adsorption capacity of Pb(II) decreases with the number of recycles, and Mn/diatomite could still exhibit approximately 55% of its original adsorption capacity in the 3rd recycle (Figure 11(b)).

Mn/diatomite after each recycle was subjected to FT-IR measurement, and it was found that the characteristic vibration bands of the diatomite modified by manganese oxide remain (Figure S8a). However, the peaks at the wavenumbers less than 470 cm^{-1} are observed only in the first recycled sample (Figure S8b). This indicates that the chemical bonding between Pb(II) and the manganese oxide adsorption sites reduces desorption. This is also the cause of the reduced adsorption capacity of the recycled samples.

4. Conclusions

The manganese-modified diatomite material was successfully prepared with the hydrothermal method from $KMnO_4$, HCl, and diatomite. The resulting Mn/diatomite possesses a high manganese content (20.47% by weight) and a large specific surface area ($S_{BET} = 68.5 \, \mathrm{m^2 \, g^{-1}}$). The manganese oxide covers the diatomite surface. Mn/diatomite can be used as an adsorbent to remove Pb(II) ions from aqueous solutions with a maximum adsorption capacity of $81.42 \, \mathrm{mg \, g^{-1}}$. The Pb(II) adsorption on Mn/diatomite is spontaneous and endothermic, with an activation energy of $41.56 \, \mathrm{kJ \, mol^{-1}}$. The material is a stable, potential adsorbent in environmental treatments.

Data Availability

The data used to support the findings of this study are available from the corresponding authors upon request.

Conflicts of Interest

The authors declare that they have no conflicts of interest.

Acknowledgments

Supplementary Materials

Figure S1: Pb(II) adsorption capacity in an aqueous solution of nano-MnO_2 samples prepared at different $KMnO_4$/HCl molar ratios: (a) 1 : 1; (b) 1 : 2; (c) 1 : 4; (d) 1 : 8 (experimental conditions: 0.1 g of adsorbent; 100 mL of Pb(II) solution with $C_0 = 70.6 \, \mathrm{mg \, L^{-1}}$). Figure S2: SEM image and EDX mapping of the nano-MnO_2 sample after Pb(II) adsorption. Figure S3: SEM image and EDX mapping of Mn/diatomite. Figure S4: SEM image and EDX mapping of Mn/diatomite after Pb(II) adsorption. Figure S5: plot depicting Pb(II) adsorption kinetics on Mn/diatomite according to the pseudo-first-order and pseudo-second-order equations: (a) at different initial concentrations of Pb(II) solutions; (b) at different adsorption temperatures. Figure S6: simulation of adsorption isotherms determined by a nonlinear method of Pb(II) adsorption on different materials: (a) Mn/diatomite; (b) natural diatomite; (c) Nano-MnO_2. Figure S7: the dependence of $\ln (k_2)$ versus $1/T$ of Pb(II) adsorption on Mn/diatomite. Figure S8: FT-IR spectra of reused Mn/diatomite samples: (a) wavenumber region 4000-400 $\mathrm{cm^{-1}}$; (b) wavenumber region 600-400 $\mathrm{cm^{-1}}$. Table S1: manganese element content and Pb(II) adsorption capacity in aqueous solution of the Mn/diatomite samples. Table S2: textural properties of diatomite samples. (Supplementary Materials)

References

[1] H. Çelebi and O. Gök, "Evaluation of lead adsorption kinetics and isotherms from aqueous solution using natural walnut shell," *International Journal of Environmental Research*, vol. 11, no. 1, pp. 83–90, 2017.

[2] H. Çelebi, G. Gök, and O. Gök, "Adsorption capability of brewed tea waste in waters containing toxic lead(II), cadmium (II), nickel (II), and zinc(II) heavy metal ions," *Scientific Reports*, vol. 10, no. 1, article 17570, 2020.

[3] H. Cao, X. Ma, Z. Wei et al., "Behavior and mechanism of the adsorption of lead by an eco-friendly porous double-network hydrogel derived from keratin," *Chemosphere*, vol. 289, article 133086, 2022.

[4] T. M. Zewail and N. S. Yousef, "Kinetic study of heavy metal ions removal by ion exchange in batch conical air spouted bed," *Alexandria Engineering Journal*, vol. 54, no. 1, pp. 83–90, 2015.

[5] M. Shafiq, A. A. Alazba, and M. T. Amin, "Removal of heavy metals from wastewater using date palm as a biosorbent: a comparative review," *Sains Malaysiana*, vol. 47, no. 1, pp. 35–49, 2018.

[6] K. C. Khulbe and T. Matsuura, "Removal of heavy metals and pollutants by membrane adsorption techniques," *Applied Water Science*, vol. 8, no. 1, p. 19, 2018.

[7] X. Yang, G. Xu, and H. Yu, "Removal of lead from aqueous solutions by ferric activated sludge-based adsorbent derived from biological sludge," *Arabian Journal of Chemistry*, vol. 12, no. 8, pp. 4142–4149, 2019.

[8] H. Li, S. Wu, C. Du, Y. Zhong, and C. Yang, "Preparation, performances, and mechanisms of microbial flocculants for wastewater treatment," *International Journal of Environmental Research and Public Health*, vol. 17, no. 4, p. 1360, 2020.

[9] Y. Zhang and X. Duan, "Chemical precipitation of heavy metals from wastewater by using the synthetical magnesium hydroxy carbonate," *Water Science & Technology*, vol. 81, no. 6, pp. 1130–1136, 2020.

[10] Y. Al-Degs, M. A. M. Khrasisheh, and M. F. Tutunji, "Sorption of lead ions on diatomite and manganese oxides modified diatomite," *Water Research*, vol. 35, no. 15, pp. 3724–3728, 2001.

[11] M. A. M. Khraished, Y. S. Al-degs, and W. A. M. Mcminn, "Remediation of wastewater containing heavy metals using raw and modified diatomite," *Chemical Engineering Journal*, vol. 99, no. 2, pp. 177–184, 2004.

[12] Y. Du, G. Zheng, J. Wang, L. Wang, J. Wu, and H. Dai, "MnO_2 nanowires in situ grown on diatomite: highly efficient absorbents for the removal of Cr(VI) and As(V)," *Microporous and Mesoporous Materials*, vol. 200, pp. 27–34, 2014.

[13] N. Caliskan, A. R. Kul, S. Alkan, E. G. Sogut, and I. Alacabey, "Adsorption of zinc(II) on diatomite and manganese-oxide-modified diatomite: a kinetic and equilibrium study," *Journal of Hazardous Materials*, vol. 193, pp. 27–36, 2011.

[14] B. Kayranli, O. Gok, T. Yilmaz et al., "Low-cost organic adsorbent usage for removing Ni^{2+} and Pb^{2+} from aqueous solution and adsorption mechanisms," *International journal of Environmental Science and Technology*, vol. 19, no. 5, pp. 3547–3564, 2022.

[15] Z. Al-Qodah, W. K. Lafi, Z. Al-Anber, M. Al-Shannag, and A. Harahsheh, "Adsorption of methylene blue by acid and heat treated diatomaceous silica," *Desalination*, vol. 217, no. 1-3, pp. 212–224, 2007.

[16] G. Zhang, D. Cai, M. Wang, C. Zhang, J. Zhang, and Z. Wu, "Microstructural modification of diatomite by acid treatment, high-speed shear, and ultrasound," *Microporous and Mesoporous Materials*, vol. 165, pp. 106–112, 2013.

[17] B. H. D. Son, V. Q. Mai, D. X. Du, N. H. Phong, and D. Q. Khieu, "A study on Astrazon Black AFDL dye adsorption onto Vietnamese diatomite," *Journal of Chemistry*, vol. 2016, Article ID 8685437, 11 pages, 2016.

[18] J. Chang, J. Zhang, B. Tan, Q. Wang, N. Liu, and Q. Xue, "New insight into the removal of Cd(II) from aqueous solution by diatomite," *Environmental Science and Pollution Research*, vol. 27, no. 9, pp. 9882–9890, 2020.

[19] Y. Liu, J. Zhang, X. Sheng, N. Li, and Q. Ping, "Adsorption and release kinetics, equilibrium, and thermodynamic studies of hymexazol onto diatomite," *ACS Omega*, vol. 5, no. 45, pp. 29504–29512, 2020.

[20] B. H. D. Son, V. Q. Mai, D. X. Du, N. H. Phong, N. D. Cuong, and D. Q. Khieu, "Catalytic wet peroxide oxidation of phenol solution over Fe-Mn binary oxides diatomite composite," *Journal of Porous Materials*, vol. 24, no. 3, pp. 601–611, 2017.

[21] D. Q. Khieu, B. H. D. Son, V. T. T. Chau, P. D. Du, N. H. Phong, and N. T. D. Chau, "3-Mercaptopropyltrimethoxysilane modified diatomite: preparation and application for voltammetric determination of lead (II) and cadmium (II)," *Journal of Chemistry*, vol. 2017, Article ID 9560293, 10 pages, 2017.

[22] M. B. Nguyen, T. V. Nguyen, G. H. Le et al., "High CO adsorption performance of CuCl-modified diatomites by using the novel method "atomic implantation"," *Journal of Chemistry*, vol. 2021, Article ID 9762578, 11 pages, 2021.

[23] T. H. Đ⬚ng, X. H. Nguyễn, C. L. Chou, and B. H. Chen, "Preparation of cancrinite-type zeolite from diatomaceous earth as transesterification catalysts for biodiesel production," *Renewable Energy*, vol. 174, pp. 347–358, 2021.

[24] P. D. Du and H. T. Danh, "Single and binary adsorption systems of rhodamine B and methylene blue onto alkaliactivated Vietnamese diatomite," *Adsorption Science & Technology*, vol. 2021, Article ID 1014354, 13 pages, 2021.

[25] A. Tavakoli, M. Sohrabi, and A. Kargari, "A review of methods for synthesis of nanostructured metals with emphasis on iron compounds," *Chemical Papers*, vol. 61, no. 3, pp. 151–170, 2007.

[26] C. Burda, X. Chen, R. Narayanan, and M. A. El-Sayed, "Chemistry and properties of nanocrystals of different shapes," *Chemical Reviews*, vol. 105, no. 4, pp. 1025–1102, 2005.

[27] D. Höllen, D. Klammer, I. Letofsky-Papst, and M. Dietzel, "Hydrothermal alteration of diatomite for removal of aqueous Cu^{2+}, Pb^{2+} and Zn^{2+}," *Materials Science and Engineering B (Solid-State Materials for Advanced Technology)*, vol. 10, pp. 523–533, 2012.

[28] H. Luo, F. Fu, and B. Tang, "Ferrous sulfide supported on modified diatomite for the removal of Cr(VI): performance and mechanism," *Colloids and Surfaces A: Physicochemical and Engineering Aspects*, vol. 670, article 131538, 2023.

[29] W. Yuan, P. Yuan, D. Liu et al., "In situ hydrothermal synthesis of a novel hierarchically porous TS-1/modified-diatomite composite for methylene blue (MB) removal by the synergistic effect of adsorption and photocatalysis," *Journal of Colloid and Interface Science*, vol. 462, pp. 191–199, 2016.

[30] Y. Xiao, W. Huo, S. Yin et al., "One-step hydrothermal synthesis of Cu-doped MnO_2 coated diatomite for degradation of methylene blue in Fenton-like system," *Journal of Colloid and Interface Science*, vol. 556, pp. 466–475, 2019.

[31] J. W. Murray, "The surface chemistry of hydrous manganese dioxide," *Journal of Colloid and Interface Science*, vol. 46, no. 3, pp. 357–371, 1974.

[32] J. Chen, J. C. Jin, V. Purohit, M. B. Cutlip, and S. L. Suib, "Photoassisted catalytic oxidation of alcohols and halogenated hydrocarbons with amorphous manganese oxides," *Catalysis Today*, vol. 33, no. 1-3, pp. 205–214, 1997.

[33] L. Mao, D. Zhang, T. Sotomura, K. Nakatsu, N. Koshiba, and T. Ohsaka, "Mechanistic study of the reduction of oxygen in air electrode with manganese oxides as electrocatalysts," *Electrochimica Acta*, vol. 48, no. 8, pp. 1015–1021, 2003.

[34] Z.-X. Chen, X.-Y. Jin, Z. Chen, M. Megharaj, and R. Naidu, "Removal of methyl orange from aqueous solution using bentonite-supported nanoscale zero-valent iron," *Journal of Colloid and Interface Science*, vol. 363, no. 2, pp. 601–607, 2011.

[35] R. Han, W. Zou, Y. Wang, and L. Zhu, "Removal of uranium(VI) from aqueous solutions by manganese oxide coated zeolite: discussion of adsorption isotherms and pH effect," *Journal of Environmental Radioactivity*, vol. 93, no. 3, pp. 127–143, 2007.

[36] S. Li, D. Li, F. Su, Y. Ren, and G. Qin, "Uniform surface modification of diatomaceous earth with amorphous manganese oxide and its adsorption characteristics for lead ions," *Applied Surface Science*, vol. 317, pp. 724–729, 2014.

[37] M. A. Al-Ghouti, Y. S. Al-Degs, M. A. M. Khraisheh, M. N. M. Ahmad, and S. J. Allen, "Mechanisms and chemistry of dye adsorption on manganese oxides-modified diatomite," *Journal of Environmental Management*, vol. 90, no. 11, pp. 3520–3527, 2009.

[38] B. Bahramian, F. D. Ardejani, V. Mirkhani, and K. Badii, "Diatomite-supported manganese Schiff base: an efficient catalyst for oxidation of hydrocarbons," *Applied Catalysis A: General*, vol. 345, no. 1, pp. 97–103, 2008.

[39] Y. X. Zhang, M. Huang, F. Li, X. L. Wang, and Z. Q. Wen, "One-pot synthesis of hierarchical MnO_2-modified diatomites for electrochemical capacitor electrodes," *Journal of Power Sources*, vol. 246, pp. 449–456, 2014.

[40] J. Wu, H. Huang, L. Yu, and J. Hu, "Controllable hydrothermal synthesis of MnO_2 nanostructures," *Advances in Materials Physics and Chemistry*, vol. 3, no. 3, pp. 201–205, 2013.

[41] N. L. M. Linh, D. H. Van, T. Duong, M. X. Tinh, and D. Q. Khieu, "Adsorption of arsenate from aqueous solution onto modified Vietnamese bentonite," *Advances in Materials Science and Engineering*, vol. 2019, Article ID 2710926, 13 pages, 2019.

[42] Y. Shao, X. Wang, Y. Kang, Y. Shu, Q. Sun, and L. Li, "Application of Mn/MCM-41 as an adsorbent to remove methyl blue from aqueous solution," *Journal of Colloid and Interface Science*, vol. 429, pp. 25–33, 2014.

[43] H. Faghihian and M. Naghavi, "Synthesis of amine-functionalized MCM-41 and MCM-48 for removal of heavy metal ions from aqueous solutions," *Separation Science and Technology*, vol. 49, no. 2, pp. 214–220, 2014.

[44] W. S. W. Ngah and S. Fatinathan, "Adsorption characterization of Pb(II) and Cu(II) ions onto chitosan-tripolyphosphate beads: kinetic, equilibrium and thermodynamic studies," *Journal of Environmental Management*, vol. 91, no. 4, pp. 958–969, 2010.

[45] A. Kamari and W. S. Wan Ngah, "Isotherm, kinetic and thermodynamic studies of lead and copper uptake by H_2SO_4 modified chitosan," *Colloids and Surfaces B: Biointerfaces*, vol. 73, no. 2, pp. 257–266, 2009.

[46] B. H. Hameed, A. A. Ahmad, and N. Aziz, "Isotherms, kinetics and thermodynamics of acid dye adsorption on activated palm ash," *Chemical Engineering Journal*, vol. 133, no. 1-3, pp. 195–203, 2007.

[47] M. Goswami, L. Borah, D. Mahanta, and P. Phukan, "Equilibrium modeling, kinetic and thermodynamic studies on the adsorption of Cr(VI) using activated carbon derived from matured tea leaves," *Journal of Porous Materials*, vol. 21, no. 6, pp. 1025–1034, 2014.

[48] O. Hamdaoui and E. Naffrechoux, "Modeling of adsorption isotherms of phenol and chlorophenols onto granular activated carbon. Part II. Models with more than two parameters," *Journal of Hazardous Materials*, vol. 147, no. 1-2, pp. 401–411, 2007.

[49] P. D. Du, N. T. Hieu, T. C. To et al., "Aminopropyl functionalised MCM-41: synthesis and application for adsorption of Pb(II) and Cd(II)," *Advances in Materials Science and Engineering*, vol. 2019, Article ID 8573451, 15 pages, 2019.

[50] A. Terdputtakun, O. Arqueropanyo, P. Sooksamiti, S. Janhom, and W. Naksata, "Adsorption isotherm models and error analysis for single and binary adsorption of Cd(II) and Zn(II) using leonardite as adsorbent," *Environmental Earth Sciences*, vol. 76, no. 22, p. 777, 2017.

[51] N. T. T. Tu, T. S. Thanh, P. T. Quy et al., "Trinary component adsorption of methylene blue, methyl orange, and methyl red from aqueous solution using TiO_2/activated carbon," *Adsorption Science & Technology*, vol. 2023, Article ID 8943198, 17 pages, 2023.

[52] J. Jin, J. Ouyang, and H. Yang, "One-step synthesis of highly ordered Pt/MCM-41 from natural diatomite and the superior capacity in hydrogen storage," *Applied Clay Science*, vol. 99, pp. 246–253, 2014.

[53] Y. Fu, X. Xu, Y. Huang, J. Hu, Q. Chen, and Y. Wu, "Preparation of new diatomite-chitosan composite materials and their adsorption properties and mechanism of Hg(II)," *Royal Society Open Science*, vol. 4, no. 12, p. 170829, 2017.

[54] P. Liu, T. Chen, and J. G. Zheng, "Removal of iodate from aqueous solution using diatomite/nano titanium dioxide composite as adsorbent," *Journal of Radioanalytical and Nuclear Chemistry*, vol. 324, no. 3, pp. 1179–1188, 2020.

[55] D. Dai, H. Liang, D. He, H. Potgieter, and M. Li, "Mn-doped Fe_2O_3/diatomite granular composite as an efficient Fenton catalyst for rapid degradation of an organic dye in solution," *Journal of Sol-Gel Science and Technology*, vol. 97, no. 2, pp. 329–339, 2021.

[56] P. Ebrahimi and A. Kumar, "Diatomite chemical activation for effective adsorption of methylene blue dye from model textile wastewater," *International Journal of Environmental Science and Development*, vol. 12, no. 1, pp. 23–28, 2021.

[57] G. Leofanti, M. Padovan, G. Tozzola, and B. Venturelli, "Surface area and pore texture of catalysts," *Catalysis Today*, vol. 41, no. 1-3, pp. 207–219, 1998.

[58] L. Feng, Z. Xuan, H. Zhao et al., "MnO_2 prepared by hydrothermal method and electrochemical performance as anode for lithium-ion battery," *Nanoscale Research Letters*, vol. 9, no. 1, p. 290, 2014.

[59] Y. Yang, L. Xiao, Y. Zhao, and F. Wang, "Hydrothermal synthesis and electrochemical characterization of α-MnO_2 nanorods as cathode material for lithium batteries," *International Journal of Electrochemical Science*, vol. 3, no. 1, pp. 67–74, 2008.

[60] P. Yuan, D. Q. Wu, H. P. He, and Z. Y. Lin, "The hydroxyl species and acid sites on diatomite surface: a combined IR and Raman study," *Applied Surface Science*, vol. 227, no. 1-4, pp. 30–39, 2004.

[61] S. C. Ma, Z. G. Wang, J. L. Zhang, D. H. Sun, and G. X. Liu, "Detection analysis of surface hydroxyl active sites and simulation calculation of the surface dissociation constants of aqueous diatomite suspensions," *Applied Surface Science*, vol. 327, pp. 453–461, 2015.

[62] C. V. Tran, D. V. Quang, H. P. N. Thi, T. N. Truong, and D. D. La, "Effective removal of Pb(II) from aqueous media by a new design of Cu–Mg binary ferrite," *ACS Omega*, vol. 5, no. 13, pp. 7298–7306, 2020.

[63] M. Pena, X. Meng, G. P. Korfiatis, and C. Jing, "Adsorption mechanism of arsenic on nanocrystalline titanium dioxide," *Environmental Science & Technology*, vol. 40, no. 4, pp. 1257–1262, 2006.

[64] T. Mahmood, M. T. Saddique, A. Naeem, P. Westerhoff, S. Mustafa, and A. Alum, "Comparison of different methods for the point of zero charge determination of NiO," *Industrial & Engineering Chemistry Research*, vol. 50, no. 17, pp. 10017–10023, 2011.

[65] A. A. Malhis, S. H. Arar, M. K. Fayyad, and H. A. Hodali, "Amino- and thiol-modified microporous silicalite-1 and mesoporous MCM-48 materials as potential effective adsorbents for Pb(II) in polluted aquatic systems," *Adsorption Science and Technology*, vol. 36, no. 1-2, pp. 270–286, 2018.